

## Ion velocity distribution measurements in a magnetized laser plasma expansion

A.B. Zylstra,<sup>a,b,1</sup> C. Constantin,<sup>a</sup> E.T. Everson,<sup>a</sup> D. Schaeffer,<sup>a</sup> N.L. Kugland,<sup>a,c</sup>  
P. Pribyl<sup>a</sup> and C. Niemann<sup>a,c</sup>

<sup>a</sup>University of California Los Angeles,  
Los Angeles, CA 90095, U.S.A.

<sup>b</sup>Pomona College,  
Claremont, CA 91711, U.S.A.

<sup>c</sup>Lawrence Livermore National Laboratory,  
Livermore, CA 94550, U.S.A.

E-mail: [zylstra@mit.edu](mailto:zylstra@mit.edu)

**ABSTRACT:** Langmuir probes are used to study the expansion of a laser plasma into a large (17 m long  $\times$  0.6 m diameter) ambient magnetized cylindrical plasma. The expansion is either perpendicular or at 45° to the 300 – 600 G axial background field. One probe geometry allows data collection close to the ablation surface, inside a diamagnetic bubble formed during the laser plasma expansion. We measure expansion velocities of this diamagnetic cavity and the bulk laser plasma. Additionally, we detect fast ions along the axis of the ambient plasma column when the laser plasma expansion is directed at 45° to the background field. We obtain the fast ion velocity distribution by comparing the measured ion gyroradii to those predicted by Monte Carlo simulations of the ion trajectories in an external magnetic field. Experimental measurement of fast ion velocity distributions can help tune the experimental parameters that are required to drive collisionless shock waves through a laboratory plasma.

**KEYWORDS:** Plasma diagnostics - probes; Plasma diagnostics - charged-particle spectroscopy

<sup>1</sup>Corresponding author. Current address: Massachusetts Institute of Technology, 77 Massachusetts Ave, NW17-256, Cambridge, MA 02139, U.S.A.

---

## Contents

<b>1</b>	<b>Introduction</b>	<b>1</b>
<b>2</b>	<b>Probe design and implementation</b>	<b>2</b>
<b>3</b>	<b>Experimental setup</b>	<b>3</b>
<b>4</b>	<b>Laser plasma expansion</b>	<b>4</b>
<b>5</b>	<b>Fast ion measurements</b>	<b>5</b>
<b>6</b>	<b>Fast ion velocity spectrometer</b>	<b>6</b>
<b>7</b>	<b>Determining charge states</b>	<b>9</b>
<b>8</b>	<b>Conclusions</b>	<b>10</b>

---

## 1 Introduction

In the 1950s R. Sagdeev proposed the existence of shock waves without collisions [1]. Later, these collisionless shock waves were observed by Ness *et al* in the Earth’s magnetosphere [2]. It has since become apparent that collisionless shock waves are fundamental astrophysical phenomena [3]. Specific examples include supernova remnants [4] and coronal mass ejections [5]; additionally, collisionless shocks are thought to be responsible for highly-energetic cosmic rays [6, 7].

Laboratory experiments have attempted to replicate the conditions necessary for collisionless shock formation [8–12] and particle acceleration with relevance to cosmic phenomena. These necessary conditions are well documented [13–15]. At the University of California, Los Angeles (UCLA) we can create unique plasma conditions by utilizing the large, magnetized plasma generated by the Large Plasma Device (LAPD) and the energetic laser plasma produced by a high-power ( $5 \times 10^{13}$  W/cm<sup>2</sup>), ns-pulse laser. Experiments with rapidly expanding (velocities of several 100 km/s) laser plasmas in the LAPD launch waves that can approach the conditions for collisionless shocks [16].

Generation of laboratory shocks requires fine tuning of the expansion velocity of the exploding laser plasma. Langmuir probes, which have traditionally been used for time-of-flight measurements [17], can provide feedback for the expansion velocity tuning. Instead of these traditional methods, this paper presents a velocity spectroscopy technique which is used to determine the ion velocity distribution. This is done by utilizing experimental Langmuir measurements in conjunction with Monte Carlo simulations of ion trajectories to determine ion velocities.

We also present novel measurements close to the ablation surface with a probe perpendicular to the expansion. This allows measurements of the laser plasma ablation velocity as well as the density.

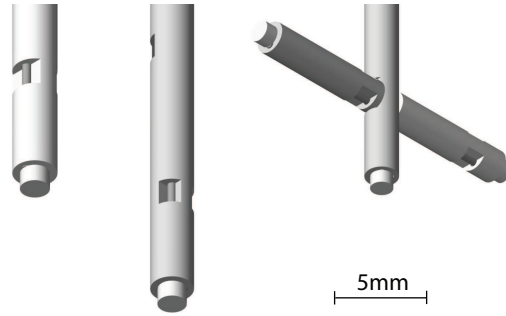


**Figure 1.** Mach Probes: from left to right: single parallel flow probe, double parallel flow probe, double perpendicular flow probe.

## 2 Probe design and implementation

These experiments used Langmuir and Mach probes with exposed areas on the order of  $1 \text{ mm}^2$ . The dual-function probe designs used can function as either a Langmuir or a Mach probe, with the analysis presented in the paper focusing on using them as Langmuir probes. Several of these probe designs are shown in figure 1. The exposed faces were either parallel or perpendicular to the probe axis. We selectively exposed sections ( $\approx 1.5 \text{ mm} \times 0.5 \text{ mm}$ ) of the inner bores of an alumina tube (2.4 mm outer diameter, 25 cm length). In the case of the perpendicular exposed face, shown on the right in figure 1, we epoxied an additional alumina arm to the main probe tube to achieve the desired geometry. We inserted small tungsten wires (0.010-0.020") through the tube bores, thereby exposing the wires to the plasma only in the cut sections. An additional alumina piece capped the end of the alumina tube. The tungsten wires were spot welded to the center conductor of coaxial cables inside the stainless steel shaft. We chose the materials for the actual probe (tungsten and alumina) for their desirable thermal stability in the harsh plasma environment.

The experimental setup is shown in figure 2. A bias between the cathode and anode mesh generates an electron cascade along the magnetic field lines that ionizes the pre-filled gas in the machine out to a radius of 30 cm. More than 400 ports were available on the LAPD chamber for experimental access. In this case, the ablation target and laser were coplanar with the plane perpendicular to the main axial field. The probes were negatively biased to approximately 70 V with respect to the anode. We measured the probe current by recording the voltage drop across a  $10 \text{ } \Omega$  resistor that was placed in series with the probe tip. This time-resolved measurement was taken with a 100 MHz, 14-bit data acquisition system (DAQ). To protect the DAQ from the probe bias and to mitigate noise due to ground loops the probe was optically isolated from the DAQ. We calibrated the frequency response of this system using a network analyzer. Since the optical isolator gain is a function of signal frequency, based on the calibration we scaled the signal amplitudes in the frequency domain during the analysis. As shown in figure 2 this correction is minimal for low frequencies but becomes significant for signals greater than  $\approx 10 - 20 \text{ MHz}$ .

Some limitations of this design included occasional spot weld failures to the tungsten wires, relatively high levels of noise due to the small exposed area, and large variation in the exposed areas. With appropriate calibrations, tests using well-characterized plasmas, and analysis methods these limitations can be mitigated, as will be shown in this work.

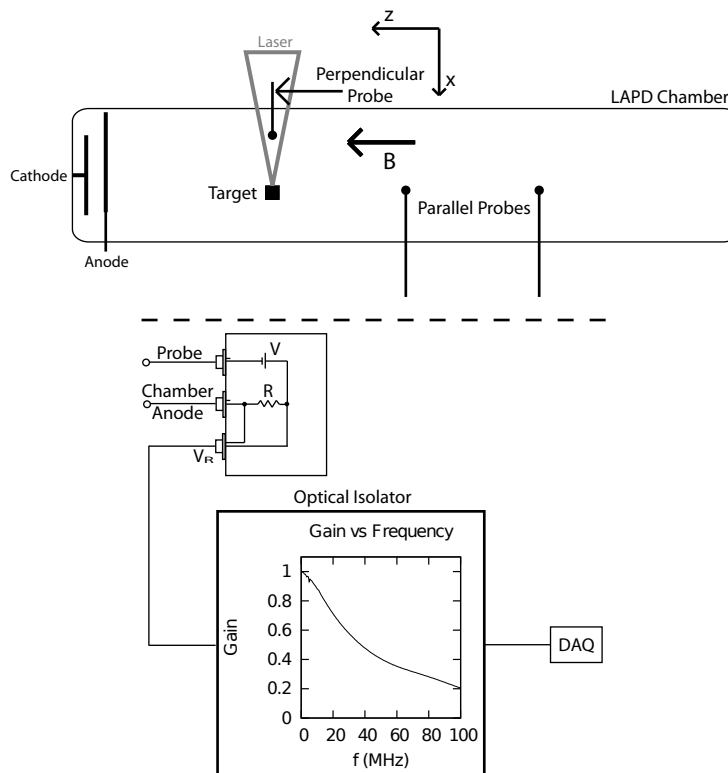


**Figure 2.** A top view of the experimental layout showing the probes (parallel and perpendicular) and target position in the LAPD chamber (top). The laser is incident on the target from above the horizontal plane. Langmuir probe circuit and optical isolator response (bottom).

### 3 Experimental setup

The LAPD [18] produced a 17 m long, 60 cm diameter plasma at a 1 Hz repetition rate. The plasma was maintained for approximately 10 ms with a nominal density of  $2 \times 10^{12} \text{cm}^{-3}$ , an electron temperature of 5 eV, and an ion temperature of 1 eV. The plasma was current free, quiescent over laser plasma timescales, highly reproducible, and strongly magnetized with a constant axial background field between 300 – 1800 G [18].

The Nd:glass laser used produced a 5 ns full width at half maximum (FWHM) pulse with 25 J of energy at a wavelength of 1064 nm, with a repetition rate of 1 shot every 3 minutes. The beam was focused onto a graphite target in the LAPD plasma with a peak intensity of  $5 \times 10^{13} \text{W/cm}^2$ . The target was vertically mounted from the top of the LAPD chamber and could both translate and rotate. The translation allowed a fresh ablation surface to be exposed for each shot, while the rotation allowed for a control of the blow-off angle between the target normal and the background field.

Langmuir probes, Mach probes (i.e. double sided Langmuir probes), and magnetic pickup coils ( $\vec{B}$  probes) were inserted from the sides of the chamber perpendicular to the target or axially downstream from the target as shown in figure 2. The perpendicular probe could be placed as close as 0.5 cm from the target using a motorized probe drive. The minimum distance was set by the precision of the probe drive and was chosen to prevent the probe tip from clipping the laser beam.

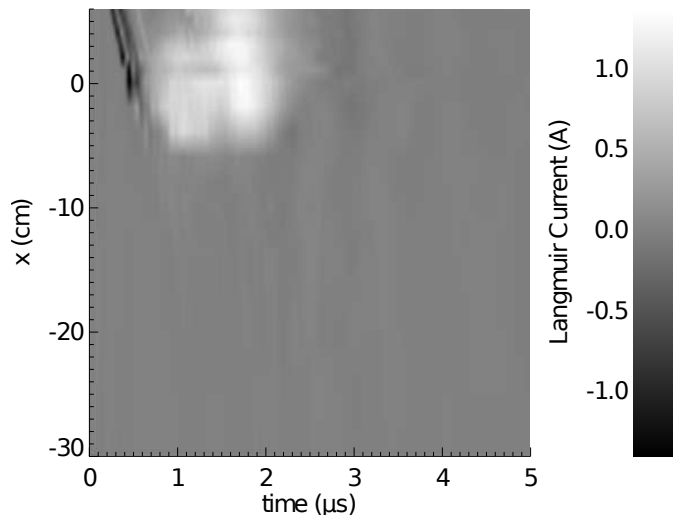


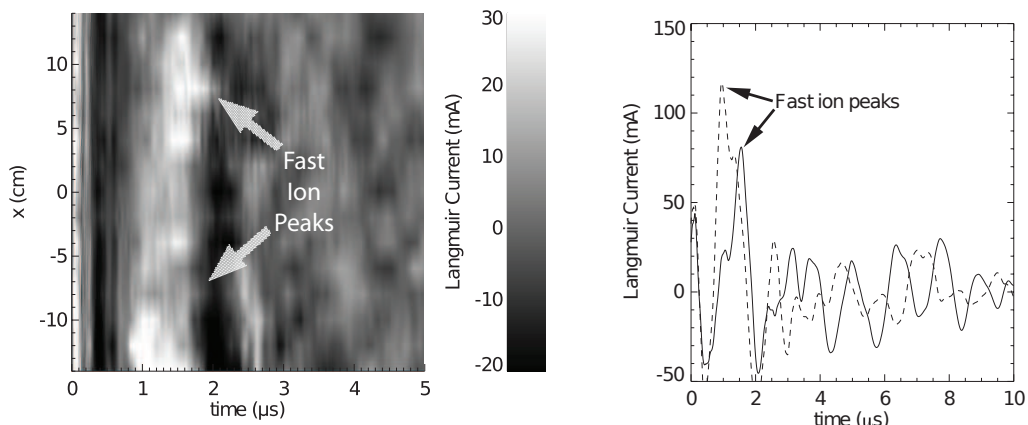
**Figure 3.** Signal versus time and probe-position as measured by the perpendicular-geometry Langmuir probe. The picture is a composite of 20 separate laser shots, each with the probe at a different position. Plasma conditions and laser energy are highly reproducible from shot to shot. The laser is focused to the target at  $x = 13$  cm (beyond the plot range) and  $t = 0$   $\mu$ s.

The perpendicular probe was either a  $\dot{B}$  probe or combination Langmuir/Mach probe. The parallel probes were a series of  $\dot{B}$ , Mach, and Langmuir probes.

#### 4 Laser plasma expansion

Figure 3 shows the signal from a perpendicular geometry Langmuir probe plotted versus time and distance from the target ( $x$ -axis in figure 2). The target surface was located at  $x = 13$  cm and the laser plasma expanded in the negative  $x$ -direction. In this geometry the face of the Langmuir probe was oriented in the  $+x$  direction with the laser plasma expansion in the  $-x$  direction. The probe signal represents the ion saturation current and is proportional to the electron density for a given temperature. The signal amplitude is plotted versus time and radial position ( $x$ -axis) with white indicating the highest density, and black the lowest. As the laser-produced carbon plasma expanded into the background plasma a diamagnetic bubble was formed [19, 20]. Under plasma conditions equivalent to those used for the Langmuir data,  $\dot{B}$  probes showed that the 300 G background field was completely expelled from the bubble. As a result, large magnetic fields were measured at the edge of the diamagnetic cavity [21]. The first signal seen on the Langmuir probe was a large negative spike, corresponding to the collection of accelerated electrons. These electrons were accelerated to energies above the bias potential by the rapidly varying electromagnetic fields.

For multiple probe locations we use a time-of-flight analysis on the Langmuir measurements to determine the expansion velocities of the leading edge of the laser plasma. At these positions we do not observe a trend that is indicative of continued acceleration. The mean expansion velocity is determined to be 269 km/s with a  $2\sigma$  error of  $\pm 23$  km/s by averaging over data from 13-19 cm from the target. Systematic timing uncertainties in the electronics (of order 10 ns) are much smaller than the several  $\mu$ s-long timescales of interest.



(a) Langmuir probe signal versus time and horizontal position. Intensity indicates signal magnitude, black to white. The picture is a composite of 30 separate target shots with reproducible plasma conditions but a different probe  $x$ -position for each shot.

(b) Langmuir current versus time at  $x = 12$  cm (solid) and  $x = -12$  cm (dashed).

**Figure 4.** Variation of the parallel geometry Langmuir probe signal with horizontal probe position  $x$ , and time. The probe is 0.65 m downstream of the target along the chamber axis. The target is at  $x = 13$  cm.

Simulations of the laser plasma expansion have been conducted using HELIOS [22], a 1-D radiation-hydrodynamics code utilizing an equation of state for carbon and the laser parameters as stated in section 3. The simulation predicts an asymptotic expansion velocity  $v \approx 270$  km/s with the velocity approaching this value within 15-20 cm of the target. This agrees well with the experimental results stated above.

We can also compute the density of the laser plasma from the data in figure 3. To do this we must assume a laser plasma electron temperature. Here we use a constant  $T_e = 25$  eV using the radiation-hydrodynamics simulation results. This is likely an overestimate of the actual number ablated, as a temperature gradient in the laser plasma would be more realistic. With this probe design a single-tip Langmuir probe is directional relative to the plasma flow (see figure 1) and an estimate must be made for the effect on the Langmuir data due to this relative motion. A probe facing towards the ablation surface will measure a higher effective density due to the flow. We estimate a total number of order  $10^{16}$  atoms ablated from the target, consistent with estimates for these laser-target parameters by empirical scaling laws [23, 24].

## 5 Fast ion measurements

In the experiment we had a number of probes sensitive to parallel velocity ions at different locations along the axis of the plasma column, as shown in figure 2. In the case where the target face was oriented at  $45^\circ$  to the background field, the laser plasma expanded normal to the target face, i.e. with a component antiparallel to the field, which allowed fast ions ablated from the target to spiral along the magnetic field lines. These fast ions were directly detected by the Langmuir probes. When the target was at  $90^\circ$  the expansion was mainly perpendicular to the field and this axial expansion was not observed.

Figure 4(a) shows a color intensity map of the fast ion signal in the case where the target is oriented at  $45^\circ$  to the background field, plotted as a function of time and probe position from the machine axis,  $x$ . In this case  $+\hat{z}$  is normal to the probe face. The probe is 0.65 m from the target along the axial direction of the chamber. The plot includes data from 30 independent laser shots with equivalent laser and plasma parameters, but different  $x$  positions. Interpolation between the data at various  $x$  positions creates the contour plot. Signal oscillations due to plasma waves are visible across the range of radial positions. These waves are also observed in data where the laser plasma expansion is perpendicular to the background field. In the present case we also see peaks in the signal between  $t = 1 - 2 \mu\text{s}$  at approximately  $x = 5 - 13 \text{ cm}$  and  $x \leq -10 \text{ cm}$ . Langmuir traces taken at positions of  $\pm 12 \text{ cm}$  radially from the chamber center are shown in figure 4(b). In these traces the fast ion peaks arrive within  $1.5 \mu\text{s}$  after the laser fires and, later in time, a plasma wave of  $\approx 0.7 \text{ MHz}$  develops, corresponding to MHD fast waves. We also note a  $0.5 \mu\text{s}$  difference in the arrival times of the ion signal peaks between the two signals, explained by simulations presented in the next section. Since this data was taken at  $z = 0.65 \text{ m}$  from the target, time-of-flight calculations give velocities of at least  $300 - 600 \text{ km/s}$ , depending on the trajectory taken. This is greater than the diamagnetic bubble expansion velocity reported in section 4.

## 6 Fast ion velocity spectrometer

With the experimental arrangement as described, the perpendicular ion energies can be determined by the Larmor radii of their trajectories, in much the same way as a mass spectrometer works. Since the target ion mass-to-charge ratio is known from CCD images, the spatial dispersion of the ions according to their Larmor radii corresponds to the velocity distribution function of the ions. The Langmuir data can be analyzed by a comparison to Monte Carlo simulations of the fast ion dynamics with a known velocity distribution. The resolution of this velocity measurement is inherently limited by the spatial resolution of the instrument in the ideal case. Most fast blow-off ions have Larmor radii ranging from  $20 - 60 \text{ cm}$ , which is much larger than the  $1 \text{ cm}$  instrumental spatial resolution. The resulting uncertainty in velocity due to the spatial resolution of the data is  $\approx 10 \text{ km/s}$ , or  $2 - 3\%$ .

A simple Monte Carlo simulation code has been developed for this analysis. The ion equation-of-motion is numerically integrated using a 4<sup>th</sup> order Runge-Kutta method. Gaussian distributions are created for the velocity, as well as the horizontal and vertical blow-off angles within a cone about the target normal. We typically simulate  $10^7$  particles with a  $1 \text{ ns}$  time step. This time step is sufficiently small for numerical convergence, which is verified by comparing with simulations at the same conditions but even smaller time steps. Using fast shutter CCD images filtered to only observe carbon spectral lines we estimate angular distributions of the blow-off as Gaussian, centered on the target normal, with  $\sigma = 15^\circ$  (half angle). Using optical filters corresponding to the lines of various charge state carbon ions we observed that the laser plasma primarily consists of  $\text{C}^{3+}$  ions.

Simulation results indicate that in shots with a relatively low ( $300 \text{ G}$ ) magnetic field and  $45^\circ$  blow-off direction, only a fraction of fast ions have gyroradii small enough to fit inside the vacuum chamber, while the rest simply collide with the chamber wall. The probe is close enough to the target to observe the ions on a wall trajectory before they collide with the wall. This leads to the

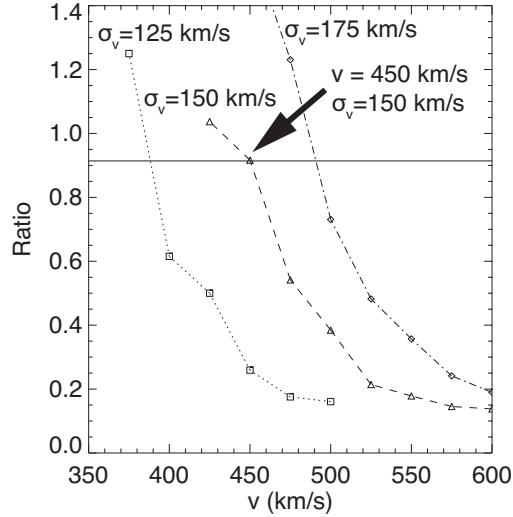


**Figure 5.** Simulated ratio of spiraling ions to ions impacting the chamber wall versus mean velocity for  $\sigma_v = 125$  km/s (dotted line),  $\sigma_v = 150$  km/s (dashed line),  $\sigma_v = 175$  km/s (dashed dotted line). The horizontal line represents the experimentally measured value.

characteristic two-peak shape observed in figure 4(a) for the following reason: the ions arriving at  $x = 5 - 13$  cm are spiraling from the target at  $x = 13$  cm whereas those with  $x \leq -10$  cm are on a trajectory to collide with the chamber wall. The different path lengths and velocities between these two groups result in the different arrival times, as observed in figure 4(a) and 4(b).

We can find a simulated mean velocity and standard deviation by comparing simulation results with experimental data. We have two criteria for establishing agreement between the measured and simulated ion velocities: the time at which laser ablated ions are detected, and the ratio of the ion populations corresponding to the two peaks in figure 4(a). The latter is done by comparing the Langmuir signals at  $x = 10$  cm to  $x = -10$  cm, which each sample the population of one group. This is shown in figure 5 as a function of mean ion velocity for three values of the velocity standard deviation,  $\sigma_v$ . The horizontal solid line represents the experimental value of the ratio. Each simulated trend fits the correct ratio for a different value of  $v$ .

We then compare the ion arrival times at these positions ( $\pm 10$  cm) to the experimental values. We want to minimize the error between the simulations and our measurements to find the best fit simulation parameters. Due to computational constraints this is done by calculating the absolute error at discrete steps in the parameters  $\bar{v}$  and  $\sigma_v$ . This is shown in figure 6 with the points from figure 5 that best agree with the experimental results plotted (+). One can see that the point with  $\bar{v} = 450$  km/s and  $\sigma_v = 150$  km/s is the best set of parameters of those simulated: the ratio is consistent with the experimental data and the average timing error is minimized. This velocity also agrees well with empirical scaling laws as applied to the experimental laser-target parameters [23, 24]. A cross-sectional plot of simulated fast ion intensity at the probe position ( $\Delta z = 0.65$  m) for these parameters is shown in figure 7(a). In figure 7(b) we integrate the simulated and experimental ion signals along the axis to show the number of particles collected versus position, with the simulation data scaled to the experimental estimate of the number of particles ablated. The qualitative trend matches reasonably well, although the experimental and simulation peak locations differ by about



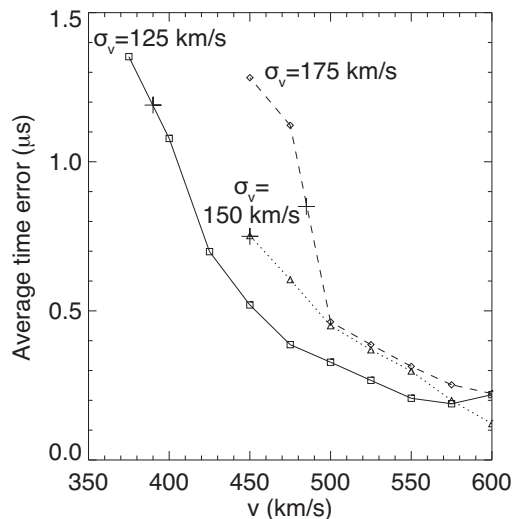
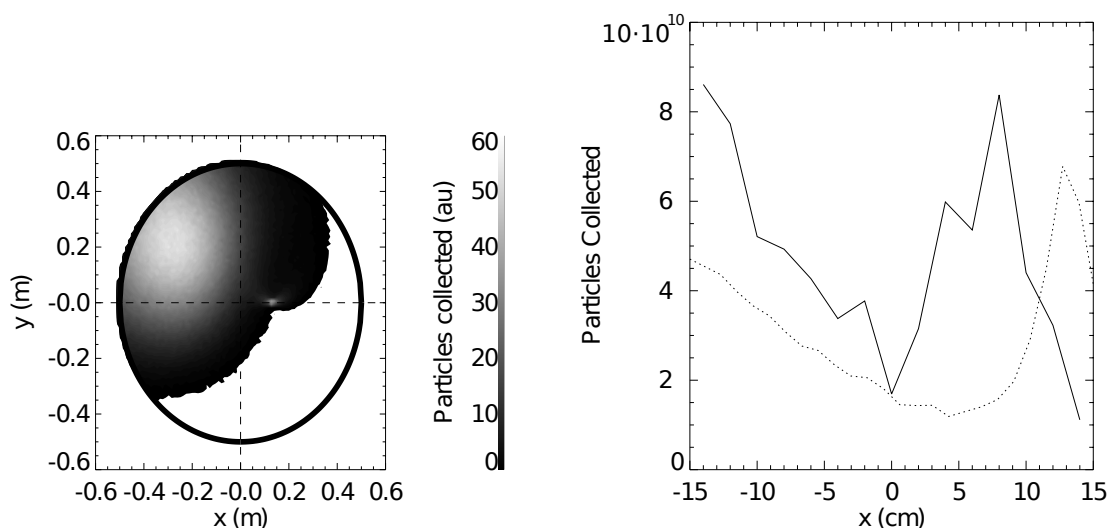


**Figure 6.** Average ion arrival time error versus velocity for  $\sigma_v = 125$  km/s (solid line),  $\sigma_v = 150$  km/s (dotted line),  $\sigma_v = 175$  km/s (dashed line). Points denoted by a + are those corresponding to the best ratio of ion populations in figure 5.



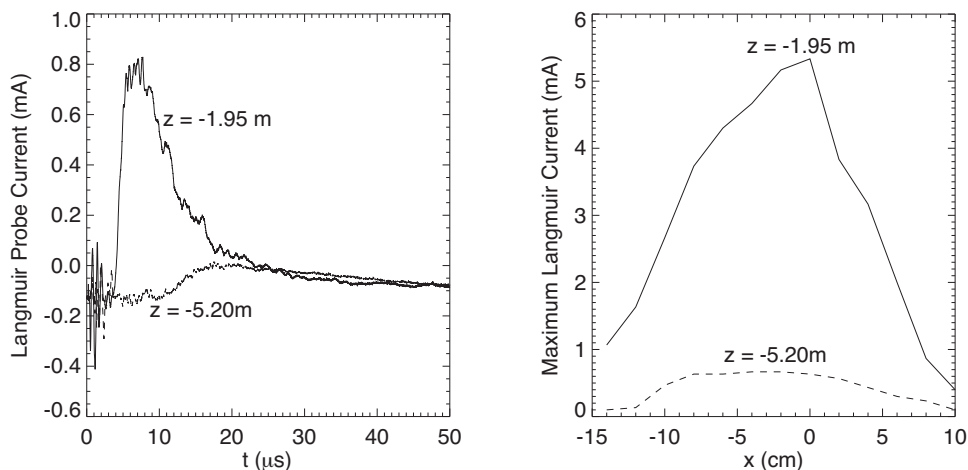
(a) Simulated fast ion intensity in a plane axially displaced by 0.65 m from the target. The color scale is in arbitrary units, with white corresponding to the highest particle flux. The Langmuir probe can be translated in the  $x$ -direction for a fixed  $y=0$  and  $y=-0.65$  m. The target is located at  $(x,y,z) = (13, 0, 0)$  cm.

(b) Integration of ion current along axis, simulation (dotted line) versus scaled experimental data (solid line). The displacement along  $x$  between the two curves is explained in the text.

**Figure 7.** Simulations of fast ion distribution for  $\bar{v} = 450$  km/s and  $\sigma_v = 150$  km/s and comparison with experimental data.

5 cm. Additional simulations indicate that this shift is likely caused by a 1 – 2 cm offset in the target vertical position from the nominal value, which is within the experimental uncertainty.

We also have data from experiments with a higher magnetic field (600 G), smaller average



(a) Probe signal versus time for two Langmuir probes axially displaced from the target at different distances.

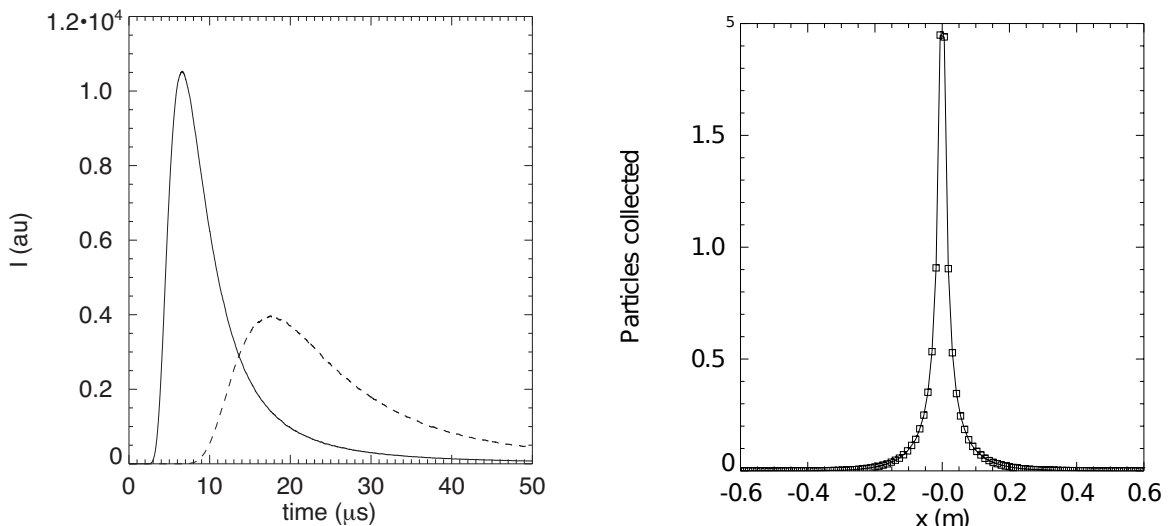
(b) Langmuir probe signal versus position along axis.

**Figure 8.** Langmuir probe data from experiments at 600 G, blow-off angle  $22.5^\circ$  relative to the external field, and reduced laser intensity ( $3 \times 10^{12}$  W/cm $^2$ ).

horizontal blow-off angle ( $22.5^\circ$ ), and reduced laser intensity ( $2 \times 10^{12}$  W/cm $^2$ ). The lower intensity results in a lower blow-off velocity. Previous time-of-flight analysis of this Langmuir data as well as Faraday cup measurements and microwave interferometer data suggest  $\bar{v} \approx 250$  km/s. Experimental data is shown in figure 8 while simulations using this pre-determined velocity are shown in figure 9. In both figures (a) shows the probe current versus time while (b) plots the probe current versus axial position. We observe very similar trends between the data and simulation in the probe current versus time comparison, although at  $z = -5.20$  m the data is relatively lower intensity than predicted by the simulation (compared to the  $z = -1.95$  m data). We believe this is because of interactions with the background plasma that were not included in the simulation model. Similarly we observe a more diffuse position profile in the data compared to the simulation. The good agreement between data and simulation in a case where the fast ion velocity is already known from independent measurements increases our confidence in the previously described velocity spectrometer method.

## 7 Determining charge states

We are also interested in determining the relative abundance of different charge states in the fast ion population. In the above low- $B$  simulations average charges in the laser plasma are estimated from CCD images, filtered to spectral lines of various carbon charge states. The average charge state is also estimated from HELIOS simulations. Our ion Monte Carlo code suggests that with the large spreads in velocity and angle of the blow-off ions in this experiment and a relatively low magnetic field field, trajectories of the separate charge populations are not sufficiently separated spatially for an accurate determination of the corresponding Larmor radii. This is because of the unfortunate coincidence that we are measuring the ion flux near to where the ions have completed an integer number of Larmor orbits.



(a) Simulated ion saturation current (particles arriving per 10ns bin) versus time for probes at  $z = -1.95\text{m}$  (solid) and  $z = -5.2\text{m}$  (dashed).

(b) Simulated Langmuir probe signal (integrated) for ions versus axial position.

**Figure 9.** Monte Carlo simulation of the ion distribution for the experiments in 600 G and  $2 \times 10^{12} \text{ W/cm}^2$ .

Further analysis of the ion tracks in the simulations suggest that measurements taken with Langmuir probes above the target plane would enable determination of the various charge states of the fast ions, since the multiply charged ions would be spatially separated due to different Larmor radii. This will be a topic of future study.

## 8 Conclusions

Using Langmuir probes we measured the expansion velocity of a diamagnetic bubble formed at the edge of the expanding laser plasma, the bulk expansion velocity of the laser plasma, and the density profile of the laser plasma several centimeters from the ablation surface. Additionally, we measured fast ions ablated from the target which spiral along the background magnetic field lines.

We introduce a method for comparing Monte Carlo simulations to the experimental data to determine a velocity distribution for these fast ions. The simulation is compared to various data sets at different blow-off parameters and magnetic fields, and is found to be in good qualitative agreement with other diagnostics. Thus, simple Langmuir probes have been used in combination with the external magnetic field of the Large Plasma Device as a velocity spectrometer for the ions in the blow-off from a laser-produced carbon plasma.

We also suggest an extension of these methods to determine the relative charge states in the fast ion population. The combination of these methods will allow detailed expansion velocity diagnostics in future experiments, which will be useful for experimental tuning in attempts to drive collisionless shock waves in the LAPD since the required energy for shock formation depends on the expansion velocities.

## Acknowledgments

This work was supported by the Department of Energy, the National Science Foundation Research Experience for Undergraduates program, and the UCLA Basic Plasma Science Facility.

## References

- [1] R. Sagdeev, *Cooperative phenomena and shock waves in collisionless plasmas*, *Rev. Plasma Phys.* **4** (1966) 23.
- [2] N. Ness, C. Scarce and J. Seek, *Initial results of the Imp 1 magnetic field experiment*, *J. Geophys. Res.* **69** (1964) 3531.
- [3] R. Sagdeev and C. Kennel, *Collisionless shock waves*, *Sci. Am.* **264** (1991) 40.
- [4] R. Enomoto et al., *The acceleration of cosmic ray protons in the supernova remnant RX J1713.7-3946*, *Nature* **416** (2002) 823.
- [5] B. Low, *Coronal mass ejections, magnetic flux ropes, and solar magnetism*, *J. Geophys. Res.* **106** (2001) 25141.
- [6] V. Berezhinskii, S. Bulanov, V. Dogiel, V. Ginzburg, V. Ptushin and V. Ginzburg, *Astrophysics of cosmic rays*, V.L. Ginzburg, Noth-Holland, Amsterdam The Netherlands (1990).
- [7] K. Koyama, R. Petre, E. Gotthelf, U. Hwang, M. Matsuura, M. Ozaki and S. Holt, *Evidence for shock acceleration of high-energy electrons in the supernova remnant SN1006*, *Nature* **378** (1995) 255.
- [8] D. Koopman and D. Tidman, *Possible observations of collisionless electrostatic shocks in laser-produced plasmas*, *Phys. Rev. Lett.* **18** (1967) 533.
- [9] J. Paul, G. Goldenbaum, A. Iiyoshi, L. Holmes and R. Hardcastle, *Measurement of electron temperatures produced by collisionless shock waves in a magnetized plasma*, *Nature* **216** (1967) 363.
- [10] B. Ripin et al., *Large-Larmor-radius interchange instability*, *Phys. Rev. Lett.* **59** (1987) 2299.
- [11] A. Bell et al., *Collisionless shock in a laser-produced ablating plasma*, *Phys. Rev. A* **38** (1988) 1363.
- [12] L. Romagnani et al., *Observation of collisionless shocks in laser-plasma experiments*, *Phys. Rev. Lett.* **101** (2008) 25004.
- [13] R. Drake, *The design of laboratory experiments to produce collisionless shocks of cosmic relevance*, *Phys. Plasmas* **7** (2000) 4690.
- [14] Y. Zakharov, *Collisionless laboratory astrophysics with lasers*, *IEEE T. Plasma Sci.* **31** (2003) 1243.
- [15] B.A. Remington, R.P. Drake and D.D. Ryutov, *Experimental astrophysics with high power lasers and Z pinches*, *Rev. Mod. Phys.* **78** (2006) 755.
- [16] C. Constantin et al., *Collisionless interaction of an energetic laser produced plasma with a large magnetoplasma*, *Astrophys. Space Sci.* **322** (2009) 155.
- [17] F. Chen, *Lecture notes on Langmuir probe diagnostics*, in *Mini-course on plasma diagnostics*, IEEE-ICOPS meeting, June 5, Jeju, Korea, June (2003).
- [18] W. Gekelman, H. Pfister, Z. Lucky, J. Bamber, D. Leneman and J. Maggs, *Design, construction, and properties of the large plasma research device — The LAPD at UCLA*, *Rev. Sci. Instrum.* **62** (1991) 2875.

- [19] M. VanZeeland, W. Gekelman, S. Vincena and G. Dimonte, *Production of Alfvén waves by a rapidly expanding dense plasma*, *Phys. Rev. Lett.* **87** (2001) 105001.
- [20] M. VanZeeland and W. Gekelman, *Laser-plasma diamagnetism in the presence of an ambient magnetized plasma*, *Phys. Plasmas* **11** (2004) 320.
- [21] E. Everson et al., *Design, construction, and calibration of a three-axis, high-frequency magnetic probe (B-dot probe) as a diagnostic for exploding plasmas*, *Rev. Sci. Instrum.* **80** (2009) 113505.
- [22] J. MacFarlane, I. Golovkin and P. Woodruff, *HELIOS-CR-A 1-D radiation-magnetohydrodynamics code with inline atomic kinetics modeling*, *J. Quant. Spectrosc. Ra.* **99** (2006) 381.
- [23] M. Key et al., *A study of ablation by laser irradiation of plane targets at wavelengths 1.05, 0.53, and 0.35  $\mu\text{m}$* , *Phys. Fluids* **26** (1983) 2011.
- [24] B. Meyer and G. Thiell, *Experimental scaling laws for ablation parameters in plane target-laser interaction with 1.06  $\mu\text{m}$  and 0.35  $\mu\text{m}$  laser wavelengths*, *Phys. Fluids* **27** (1984) 302.